YTUP

Journal of Thermal Engineering
https://jten.yildiz.edu.tr/
https://doi.org/10.47481/jten.0075

RESEARCH ARTICLE

Numerical simulation of turbulent non-premixed diffusion flame using probability density function combustion model

Said Nechad[1,2], Ali Khelil[3,*], Youcef Bouhamidi[4,5]

[1]Military Academy of Cherchell, Tipaza, 42002, Algeria
[2]University of Chlef, Laboratory of Control, Testing, Measurement and Mechanical Simulation, Chlef, 02000, Algeria
[3]University of Chlef, Laboratory of Control, Testing, Measurement and Mechanical Simulation, Chlef, 02000, Algeria
[4]Military Academy of Cherchell, Tipaza, 42002, Algeria
[5]University of Chlef, Laboratory of Control, Testing, Measurement and Mechanical Simulation, Chlef, 02000, Algeria

Abstract

The current study examines the effect of chemical reaction mechanisms on prediction of thermal and dynamic fields in the combustion process. The computational domain is a confined combustor that is equipped with a coaxial swirling burner and radial fuel injection. The general aim is to enhance the numerical prediction of the swirling diffusion flames. Turbulence chemistry interaction is modulated by the RSM turbulence model, eddy dissipation, and PDF combustion models. The three-dimensional simulations are performed by a CFD tool and discredited by the finite volume method. The numerical results validated with experimental data indicate that the PDF model gives a more accurate prediction of maximum flame temperatures with a relative error of 1.07% versus 4.07% for the eddy dissipation model. These results demonstrate the ability of the RSM-PDF combination to resolve velocity, temperature, and species distributions and, hence, to contribute to more accurate combustion modeling for other industrial applications.

Keywords: Chemical kinetics models, turbulent reacting flows, coaxial burner, diffusion flame, PDF model, CF

Cite this article as: Nechad, S., Khelil, A., & Bouhamidi, Y. (2026). Numerical simulation of turbulent non-premixed diffusion flame using probability density function combustion model. Journal of Thermal Engineering, 12(5), 1929–1942. https://doi.org/10.47481/jten.0075

1. Introduction

In modern technology, non-premixed turbulent combustion is crucial in industrial furnaces, gas turbines, diesel engines, and burners [1]. In such kind of combustion two fluids are injected separately into the combustion chamber. The chemical reaction takes place only at the interface, where they mix by molecular and turbulent diffusion. Diffusion flames have gained the interest of researchers to optimize the combustion process to address the current challenges in energy and environment. Improvement of the combustion process can make the operation more stable and reliable, and it can increase the power output and reduce fuel consumption [2]. This diffusion flame is significant because it directly improves energy efficiency and reduces polluting emissions. The Kyoto Protocols have increased the need to control the production of deleterious gases, especially pollutant emissions (carbon monoxide, nitrogen oxides and sulfur oxides) to protect the environment [3–5]. Numerical simulation tools are now an indispensable tool for reducing the cost and duration of studies, offering a reliable way to study complex combustion processes [6, 7]. The prediction of dynamic and thermal fields by means of CFD tools has been analyzed by several authors [8–12]. Frassoldati et al. [12] modeled a confined highly swirling non-premixed natural gas flame using Fluent 6.0, complying with Schmittel et al. [13]. Beck et al. [14] studied detailed chemical kinetics, especially the production of the CH radical, to determine reaction zones and the formation of the pollutant species NO. The PDF methods have made considerable progress since the 1980s and provide a suitable approach to modeling turbulent combustion [15,16]. These approaches lead to an improved performance as compared to simple conserved scalar formulations for the treatment of nonlinear source terms in combustion [17]. Repp et al. [18] studied the numerical prediction of

*Corresponding Author
E-mail Adress: a.khelil@univ-chlef.dz

Submitted: 13 January 2025; **Accepted:** 15 July 2025

This paper was recommended for publication in revised form by Editor-in-Chief Ahmet Selim Dalkılıç

thermal and dynamic fields of confined methane swirling diffusion flame. The coupling of turbulence with chemistry was handled by two probability density function (PDF) methods (Monte Carlo composition and the assumed β function) together with simple chemical reaction schemes and second-order turbulence models. The authors proved the efficiency of the Monte Carlo PDF method connecting turbulence with chemical reactions. Khelil et al. [19] achieved 3D numerical prediction study of a swirling diffusion flame. The computational domain is gas turbine combustor. The flow and complex interactions between turbulence and chemistry have been studied using the RSM model, PDF, and laminar flamelet models. These calculations allowed the reproduction of thermal behavior and the evolution of concentrations of chemical species as a function of different variables. Finally, the study validates the combination of these models (RSM, PDF and flamelet) for an accurate description of the dynamic and thermochemical fields. Zhou et al. [20] used the standard k-ε turbulence model with Rodi's correction to simulate turbulent non-premixed hydrogen-air flames. They used the CHEMKIN-II code to calculate detailed chemical kinetics for the turbulence chemistry interaction. They found that numerical results are very sensitive to turbulent diffusion coefficients used in chemical species and energy equations. Khelil et al. [21] numerically investigated a confined natural gas diffusion flame. The flow is highly turbulent. The authors combined the RSM turbulence model with the PDF method with the β function (chemically balanced reaction scheme of 9 species and 8 reactions). This was done to model the complex combustion process. The direct comparison with experimental data allowed to quantify polluting emissions and to analyze the effect of different parameters on combustion. The RSM and K-ε turbulence models align well with experimental data, as demonstrated by German et al. [22]. However, the RSM model was better in predicting some flow and flame characteristics. Boushaki et al. [23, 24] and Merlo et al. [25, 26] examined the enriching oxygen in the swirling diffusion flames of methane-air. An experimental and numerical study by Mansouri and Boushaki [27] examined a turbulent, isothermal, reactive CH4/air flame with a global equivalency ratio (ϕ) of 0.8 and high swirl number (Sn = 1.4). The study was related to the flow behavior by using RANS (Reynolds-Averaged Navier-Stokes) equations and the DDES (Delayed Detached Eddy Simulation) model [28, 29]. Three-component volumetric velocimetry (V3V) was utilized for experimental measurements in a coaxial swirling burner. The present results on the flow field exhibit strong concordance with the stereo-PIV measurements performed earlier [30–33]. Recently industrial burner designs have been directed towards aerodynamic improvements for better combustion systems. Techniques of geometric flame stabilization have been employed to intensification gas residence time of gas by taking advantage of wake effects or swirling reactive flows, such techniques as bluff-body burners [34-37] and swirl burners [38-45]. Mahmood and Saleh [46–48] in several experimental studies on premixed flames in swirl burners showed that the simultaneous optimization of several parameters leads to a significant improvement in flame stability. The parameters studied are the swirl number (S), the bluff-body geometry and the composition of the liquefied petroleum gas (LPG). These results emphasize the importance of a systemic approach, integrating aerodynamic parameters and fuel chemical properties, for the advancement of more robust combustion systems. Eldrainy et al. [49] numerically simulated the dynamic flow in a novel burner for the gas turbine combustion chamber. They confirmed the idea of variable swirl numbers at constant mass flow rates. Gang et al. [50] Compared a novel design of lobed injector with a standard swirl burner. They determined that the new injector was better at stabilizing the flames, reducing the flame volume and shifting the main flame front downstream. The accurate prediction of the complex turbulence chemistry interaction and heat release in highly turbulent diffusion flames remains a significant difficulty, despite the advances in turbulent combustion research. Most studies so far have been limited to low-turbulence flows or have ignored the complexity by using simplified models. In doing this they often ignore the contribution using advanced turbulence models like (RSM) models together with detailed combustion schemes. Moreover, there are few studies comparing the combustion models, for example the eddy dissipation model, with the PDF approach for the confined and high-intensity natural gas burners. This study fills this gap by evaluating the predictive performance of these two combustion models in combination with RSM models against experimental data, providing new insights into temperature distribution, species concentration and recirculation dynamics. The results contribute to the improvement of the reliability of the model for industrial furnace and boiler applications, where flame stability and energy efficiency are critical. Reactive turbulent flows in a restricted rapidly whirling natural gas diffusion flame are studied in this work. With a 25-kW combustion chamber, simulations and analysis are done. This paper examines how reaction processes affect numerical estimates of flow parameters, temperature, and chemical species concentrations. To achieve the precision of the numerical model, the 3D simulations were rigorously validated against experimental data, comparing the combustion models the (EDM and PDF), coupled with turbulence model (RSM). This work relates to industrial furnaces and boilers. The work suggests possible improvements to combustion models for energy efficiency and flame stability in industrial applications.

2. Problem description and mathematical modelling

The CFD has become a tool of indispensable, providing a predictive insight, as well as an economic way to optimize the design of combustion systems. This study reports on a 3D modeling of a confined swirling turbulent flow configuration (25 kW power), whose experimental configuration was analyzed in previous work [23, 25 and 27]. The experimental setup consists of a coaxial burner featuring swirling radial injection, designed for realistic operating circumstances. [25]. The associated experimental data provides a strong basis for validation of numerical models, and thus, enhances the credibility of numerical simulations in combustion process. [27].

2.1. Burner and combustion chamber

The configuration chosen is a coaxial swirl burner, previously used in the experimental works of Olivani et al. [51] and Merlo et al. [25, 26]. The burner consists of two coaxial tubes (Figure 1a). The oxidizer (air) flowing in the annular passage at the position h = −60 mm upstream of the outlet generates a swirl generator in the annular passage and thus a rotational flow. The annular section has an outer diameter of 38 mm. The middle tube has an outer diameter of 15 mm and an inner diameter of 12 mm and carries the methane to the injector head at its end (Figure 1b). The injector head has eight radial holes, equally distributed, with diameter 3 mm and 1 mm before the burner exit plane (see Figure 1b). The holes in the tube periphery to optimize the fuel-oxidant mixture and to improve the combustion efficiency. Figure 1c shows 3D view of the swirled burner. It is equipped with eight guide vans inclined at. The thickest guide vans have been reduced to 1mm to minimize the blocking effect on the flow.

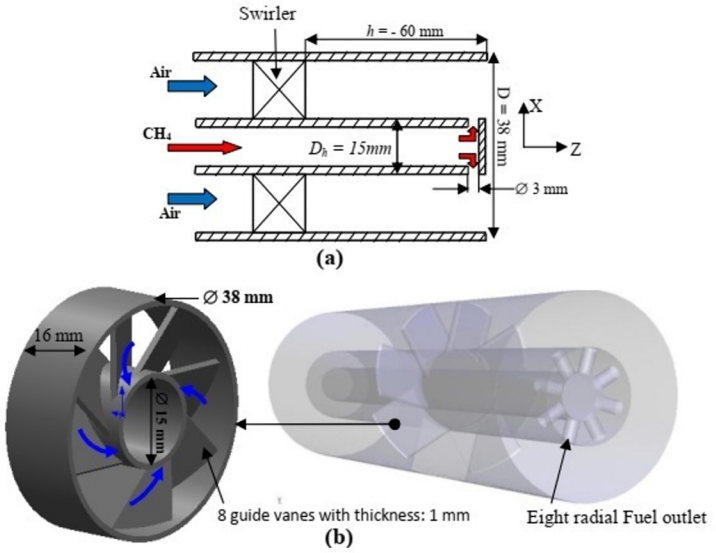

Figure 1. 2D view of burner dimensions **(a)** and 3D view of the swirled burner **(b)**

The rotational intensity, a key parameter for controlling swirling flows, is typically expressed using the swirl number, denoted as S_n. A higher S_n value implies a greater rotational intensity of the flow. The swirl number relates the tangential momentum fluxes G_θ and axial momentum fluxes G_x, according to the following formula [25]:

$$S_n = \frac{G_\theta}{RG_x} \quad (1)$$

where R is an equivalent radius.

The geometric swirl number (S_n) corresponding to this swirler configuration permitted to generate swirl intensity defined as follows [25]:

$$S_n = \frac{1}{1-\psi}\cdot\left(\frac{1}{2}\right)\cdot\frac{1-(R_h R)^4}{1-(R_h R)^2}\tan\alpha_0 \quad (2)$$

Where:

α_0 is the blade angle and ψ is the blockage factor. R and R_h correspond to both nozzle and vane pack hub radii respectively [23-27]. For instance, S_n = 1.4 corresponds to: R=17.5 mm, R_h= 8.8 mm, α = 60° and ψ= 0.23. The blocking factor (ψ) depends on the thickness and the number of blades, as defined [30]:

$$\psi = \frac{z.s}{2\pi R_h \cos(\alpha)} \quad (3)$$

where s is the blade thickness and z is the number of blades.

Three-dimensional numerical predictions are performed in a confined combustion chamber with a nominal power of 25 kW at atmospheric pressure. The chamber has a square cross-section of 48 × 48 cm² and a height of 1 meter. Merlo et al. [25,26], Boushaki et al. [24], and Mansouri et al. [27] have all provided extensive descriptions of the burner and combustion chamber. The calculations are carried out with a swirl number S_n of 1.4 and an overall equivalence ratio Φ of 0.8.

2.2. Turbulence modeling

Modeling turbulent flows demands using appropriate methodologies to account for the impact of velocity fluctuations and scalar variables on conservation equations. The density-weighted Favre-averaged equations, which present the conservation of momentum and mass in steady turbulent flows, are given below [21,49]:

$$\frac{\partial}{\partial x_j}(\bar{\rho}\tilde{u}_j) = 0 \quad (4)$$

$$\frac{\partial}{\partial x_j}(\bar{\rho}\tilde{u}_i\tilde{u}_j) = -\frac{\partial \bar{P}}{\partial x_i} - \frac{\partial(\overline{\rho u''_i u''_j})}{\partial x_j} + \frac{\partial}{\partial x_j}\left[\mu\left(\frac{\partial \tilde{u}_i}{\partial x_j} + \frac{\partial \tilde{u}_j}{\partial x_i}\right)\right] \quad (5)$$

The terms $\tilde{u}_i$ and u_i'' respectively represent the components of the Favre-averaged velocity (density-weighted average) and the associated fluctuations in the direction. The quantities $\bar{P}$ and $\bar{\rho}$ correspond to the unweighted mean pressure and density (classical time-averaged values) of the mixture, while μ denotes the laminar viscosity [12]. The terms $\bar{\rho}\overline{u''_i u''_j}$, which represent the Reynolds stresses (also known as turbulent momentum flux), are determined using the RSM turbulence model [52,53].

2. 2. 1. The RSM turbulence model

The RSM turbulence Model is an advanced methodology for modeling turbulent flows. The approach involves explicitly solving a transport equation for each individual term of the Reynolds stress tensor $\bar{\rho}\overline{u''_i u''_j}$. Unlike models based on the turbulent viscosity hy-

pothesis, such as the k–ε model, the RSM abandons the assumption of turbulence isotropy, allowing for a more accurate representation of anisotropic phenomena and complex interactions in turbulent flows. The RSM turbulence model determines the Reynolds stresses $\overline{u''_i u''_j}$ using transport equations. The individual Reynolds stresses are used to close the equation (5), which takes the following general form [22]:

$$\frac{\partial}{\partial x_k}(\bar{\rho}\tilde{u}_k \overline{u''_i u''_j}) - \frac{\partial}{\partial x_k}\left(\mu_t \frac{\partial \overline{u''_i u''_j}}{\partial x_k}\right) = P_{ij} + \Pi_{ij} - \bar{\rho}\tilde{\varepsilon}_{ij} + G_{ij} \quad (6)$$

Convection, diffusion, production, pressure-strain correlation, viscous dissipation, and extra stress production are listed from left to right. Convection and production are accurate, while all other parameters need modeling. The production term P_{ij}, can be written as follows [21]:

$$P_{ij} = -\bar{\rho}\overline{u''_i u''_k}\frac{\partial \tilde{u}_j}{\partial x_k} - \bar{\rho}\overline{u''_j u''_k}\frac{\partial \tilde{u}_i}{\partial x_k} \quad (7)$$

The turbulent diffusion term is modeled using a standard gradient diffusion hypothesis, assuming an isotropic turbulent viscosity. [22]. The turbulent viscosity μ_t is expressed by the following relation [21]:

$$\mu_t = C_\mu \bar{\rho}\frac{\tilde{k}^2}{\tilde{\varepsilon}} \quad (8)$$

Where ε is the dissipation rate of k, $\tilde{k} = \overline{u''_i u''_j}/2$ is the turbulent kinetic energy, and $C_\mu = 0.09$ is an empirical constant. The dissipation rate and turbulent kinetic energy are calculated by solving their modeled transport equations. The viscous dissipation stress term is approximated by the isotropic dissipation rate of turbulent kinetic energy as follows [21]:

$$\tilde{\varepsilon}_{ij} = \frac{2}{3}\delta_{ij}\tilde{\varepsilon} \quad (9)$$

The pressure deformation correlation term, Π_{ij}, can be expressed as [19,21]:

$$\Pi_{ij} = -C_1\bar{\rho}\frac{\tilde{\varepsilon}}{\tilde{k}}\left(\overline{u''_i u''_j} - \frac{2}{3}\delta_{ij}\tilde{k}\right) - C_2\bar{\rho}\left(P_{ij} - \frac{1}{3}\delta_{ij}P_{kk}\right) \quad (10)$$

Where C_1 and C_2 are empirical constants of the model, with values taken from [48] and equal to 1.8 and 0.6, respectively. The contribution of the additional stress production term (G_{ij}) is small compared to the other terms in equation (6) and is therefore neglected in this study according to Khelil et al. [21] and German et al. [22]. Consistent with the RSM turbulence model framework, the dissipation rate $\tilde{\varepsilon}$, is computed via its corresponding transport equation. Conversely, the turbulent kinetic energy $\tilde{k}$, does not require a separate transport equation, as it is extracted directly from the trace of normal stresses.

2. 3. Combustion models

The modeling of non-premixed flames relies on solving transport equations for one or more conserved scalars, such as the mixture fraction. Unlike explicit methods, the equations governing individual chemical species are not solved directly. Instead, the turbulence chemistry interaction is captured using two combustion models: the Eddy Dissipation Model (EDM), which ties reaction rates to turbulent scales and the PDF model, which statistically describes local fluctuations in chemical composition. These models are detailed in the subsequent section.

2. 3. 1. Eddy Dissipation Model (EDM)

The EDM is founded on the notion of Eddy Break-Up (EBU) developed in the 1970s by Spalding [54] for calculating premixed flames. Magnussen et al. [9,55] later extended in this concept to non-premixed flames. The model presents a one or two-step reaction, involving a reasonable calculation time and the reaction rate is controlled by turbulence. The average reaction rate is inversely proportional to the mixing time. This characteristic of large-scale turbulence is independent of chemical kinetics. The average net production/destruction rate of species i in reaction r can be given as follows: [27]:

$$R_{i,r} = \nu_{i,r} M_{\omega,i} A\rho\frac{\varepsilon}{k}\min\left(\frac{Y_C}{\nu_{R,r}M_{\omega,C}}\right) \quad (11)$$

$$R_{i,r} = \nu_{i,r} M_{\omega,i} AB\rho\frac{\varepsilon}{k}\left(\frac{\sum_P Y_P}{\sum_j^N \nu_{j,r}M_{\omega,j}}\right) \quad (12)$$

Where $\nu_{i,r}$ Stoichiometric coefficient of species in reaction r, $M_{\omega,j}$ is the molecular weight of species i, $\nu_{R,r}$ Stoichiometric coefficient of the limiting reactant, ρ is the density of the mixture, Y_C is the mass fraction of a reactant species c, Y_p is the mass fraction of any product species P, ε turbulent dissipation rate , k turbulent kinetic energy and The model constants A=4 and B=0.5.

2. 3. 2. Probability Density Function

The PDF approach is founded on the concept of mixture fraction. The fuel and the oxidizer mix once injected into the chamber. The final distribution is then represented by the fraction f The mixing fraction measures the quality of mixing between the two components of the fuel and the oxidant [19,52]:

$$f = \frac{Y_i - Y_{i,ox}}{Y_{i,fuel} - Y_{i,ox}} \quad (13)$$

Here, Y_i : i species mass fraction. and f = 1 in the initial fuel jet and f = 0 in the oxidizer jet. $\bar{f}$: mean mixture fraction and $\overline{f''^2}$:the mixture fraction variance is given by [19]:

$$\frac{\partial(\bar{\rho}\bar{u}_j\bar{f})}{\partial x} = \frac{\partial}{\partial x_j}\left(\frac{\mu_t}{\sigma_t}\frac{\partial \bar{f}}{\partial x_j}\right) + S_f \quad (14)$$

$$\frac{\partial(\bar{\rho}\bar{u}_j\overline{f''^2})}{\partial x} = \frac{\partial}{\partial x_j}\left(\frac{\mu_t}{\sigma_t}\frac{\partial \overline{f''^2}}{\partial x_j}\right) + C_g\mu_t\left(\frac{\partial \bar{f}}{\partial x_j}\right)^2 - C_d\rho\left(\frac{\varepsilon}{k}\overline{f''^2}\right) + S_f \quad (15)$$

$$f'' = f - \bar{f}$$

the constants $\sigma_t = 0.85$, $C_g = 2.86$, $C_d = 2.0$ and $S_f = 0$ (see [52]).

2. 4. Chemical models

In this study, methane (CH_4) combustion is analyzed using two different chemical kinetics models, which are compared. The simplified two-step chemical kinetics model is adopted in this first study, which is based on volumetric reactions. This scheme includes an initial irreversible step of fuel oxidation because of the creation of H_2O and CO, followed by a reversible step representing the CO/CO_2 equilibrium [19]:

$$2CH_4 + 3O_2 \longrightarrow 2CO + 4H_2O \quad (16)$$

$$2CO + O_2 \rightarrow 2CO_2 \quad (17)$$

The quasi-global reaction scheme is adopted in the second model developed by Westbrook et al. [56]. The species compositions analyzed in this part of the study and detailed comparison of both combustion models are presented in Table 1 and table 2 respectively. Our choice of these two models for the study of chemical kinetics is primarily based on evaluating the impact of chemical complexity on the results, as well as the need to identify the model best suited for turbulence-chemistry interactions.

Table 1. Chemical reaction mechanism

Fuel species	Oxidizer species	Reactions, Westbrook et al. [56]
95.5% CH_4, 1.7% C_2H_6, 0.1% C_3H_8, 0.1% C_4H_{10}, 0.3% CO_2 and 1.3% N_2	21% O_2 and 79% N_2	(1) $CH_4 + 1/2, O_2 \rightarrow CO + 2H_2$ (2) $CO + OH \leftrightarrow CO_2 + H$ (3) $H + O_2 \leftrightarrow O + OH$ (4) $O + H_2 \leftrightarrow H + OH$ (5) $H_2 + OH \leftrightarrow H_2O + H$ (6) $OH + OH \leftrightarrow O + H_2O$ (7) $O_2 + M \leftrightarrow O + O + M$ (8) $H + H + M \leftrightarrow H_2 + M$

Table 2. Detailed comparison of both combustion models

Criteria	EDM (6 species and 2 reactions)	PDF (9 species and 8 reactions)
Basic principle	Reaction is controlled by turbulent mixing (vorticity)	Uses a probability density function to model scalar fluctuations.
Number of reactions	2 reactions (1 irreversible, 1 reversible).	1 global reaction + 7 detailed reactions (total: 8)
Species included	CH_4, O_2, CO, CO_2, H_2O (5 species).	(CH_4, O_2, CO, CO_2, H_2, H_2O, OH, O, H 9 species, including radicals).
Chemical detail	Ignores radicals (OH,O,H) and reactive intermediates.	Includes critical radicals (OH,O,H) to describe elementary combustion mechanisms.
CO / CO_2 Equilibrium	Modeled via a simplified reversible reaction (thermodynamic approach)	Described by elementary radical-dependent reactions (e.g., $CO + OH \rightarrow CO_2 + H$).
Accuracy	Underpredicts radical-dependent processes (e.g., flame speed, NO_x formation).	Better captures intermediate steps (e.g., CO oxidation via OH), improving species predictions.
Computational Cost	Low (ideal for rapid simulations or simple systems).	Moderate to high (requires more resources for elementary reactions and radicals).
Typical applications	Preliminary studies, laminar systems, major species analysis (CO_2, H_2O)	Turbulent flames, pollutant prediction (CO, NO_x), flame stability analysis.

3. Calculation procedure

In this investigation, the CFD is employed to examine the reactive, non-premixed, swirling turbulent flow in a combustion chamber (25 Kw). The governing equations describing this reactive flow are solved using ANSYS-FLUENT. This code offers a variety of solution methods, combustion and turbulence models. To predict the combustion process, the RSM turbulence model is combined with the Eddy Dissipation (ED) approach, and the PDF β-function combustion models have been tested. The latter requires generating a look-up table via the prePDF preprocessor, incorporating the complete chemical kinetic mechanism and relevant thermodynamic data. In addition, the concentrations of O and hydroxide OH are calculated by using a predetermined PDF in temperature and a partial equilibrium.

The fuel is approximated as consisting of 100% CH_4, with negligible contributions from other components (C_2H_6, C_3H_8, C_4H_{10}). The thermal properties of the chemical species are expressed as functions of temperature. Additionally, the PRESTO and SIMPLE algorithms we used for pressure-velocity coupling and pressure interpolation, respectively. Finally, the inlet pressure was set to 101,000 Pa (1atm).

3. 1. Computational boundary conditions

When it comes to the computational domain, the boundary conditions that are described are determined by the nature of each boundary, which may be either a fluid intake, a fluid outlet, or a solid wall and pressure outlet (see Figure 2). At the fluid inlets, specific values are imposed for absolute velocity, temperature, composition, and turbulence characteristics, with predefined turbulence intensity values. Based on the Reynolds number (Re) calculation for air, the turbulence intensity values (I_{tur} in %) for the oxidant and fuel were determined (see Table 2). Through the utilization of the relation that is shown in the Fluent 6.0 User's Guide [52], it is possible to estimate the intensity of turbulence for pipe flows.

$$I_{tur} = 0.16\left(Re_{Dh}\right)^{-1/8} \quad (18)$$

For each type of boundary, several variations of conditions exist. Only those relevant to our study are described in Table 3.

Table 3. Summary of boundary condition parameters [27 and 30]

Parameters	Air	Methane CH_4
Hydraulic diameter, D_{hyd} (m)	0.023	0.012
Turbulent intensity, I_{tur} (%)	5	6
Velocity inlet (m/s)	4.6	6.0
Reynolds number	7000	1220
Temperature inlet (K)	300	300
Global equivalence ratio, Φ	0.8	
Swirl number, S_n	1.4	
Walls	Constant temperature for the chamber walls (T_{wall} = 573.15 K) with no-slip conditions.	
Outlet	Pressure outlet	
Underrelaxation	Pressure = 0.3, Density = 0.8, Energy = 1, Other parameters =0.7	
Convergence criteria	Energy=10^{-6}, Other parameters=10^{-3}	

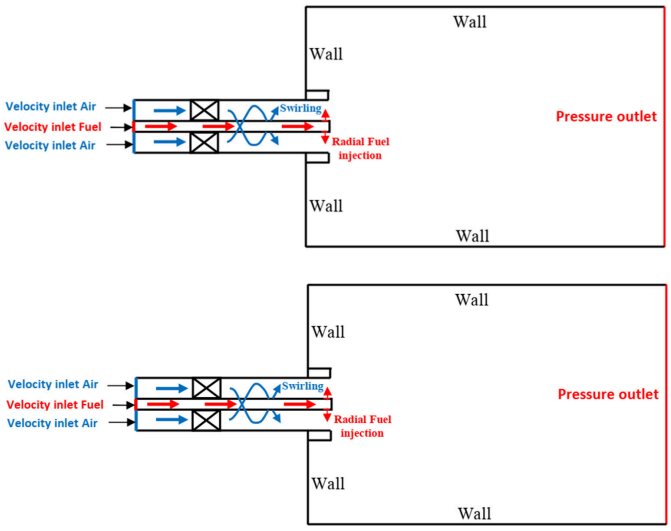

Figure 2. Schematic of the swirled non-premixed burner with Boundary conditions

3. 2. Mesh generation

The mesh was generated using a four-node tetrahedral mesh comprising a total of 2,938,901 cells. Special refinement was applied in the areas near the burner outlet (38,901 cells) to predict the various physical phenomena in these regions (see Figure 3a), particularly velocity and temperature gradients where needed. This approach also helps optimize computational effort and time (see Figure 3b).

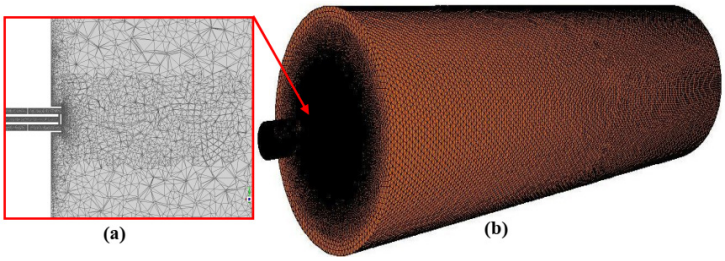

Figure 3. Computational domain grid: **(a)** Mesh refinement visualization near the coaxial burner exit, **(b)** Combustion chamber

3. 2. 1. Mesh independency

This mesh convergence study examines four grid refinements (see table 4), showing axial velocity stabilizes at approximately from Grid 2 onward, closely aligning with experimental data (7.94 m/s). The error decreases from 8.94 % for Grid 1 to approximately 5.5% for Grids 2–4. Tests with up to 3.5 million cells show no significant improvement in prediction accuracy beyond Grid 2, confirming mesh independence (≅5.5% error). Grid 1's coarse mesh yields high errors, while Grids 3 and 4 provide negligible improvements over Grid 2, which offers optimal balance of accuracy (5.53% error) and computational efficiency (2.9 million cells). The solution's insensitivity to further refinement beyond Grid 2 validates mesh independence, making Grid 2 or Grid 3 the cost-effective choice for simulations. Additional refinement increases computational cost without improving results. Analysis across different meshes (see Figure 4) confirms that the axial velocity solution remains stable at approximately 5.5% error, solidifying the conclusion of mesh independence.

Table 4. Mesh independence test

No.	Cases	Cells	Nodes	Axial velocity (m/s)	Error percentage (%)
1	Mesh 1	2,2985,97	497,642	8.650	8.94
2	Mesh 2	2,938,901	618,505	7.501	5.53
3	Mesh 3	3,462,881	715,987	7.500	5.54
4	Mesh 4	3,528,289	733,845	7.498	5.56

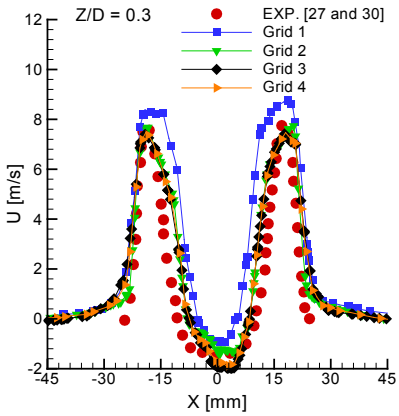

Figure 4. Mesh independency of the solution for the variation of axial velocity determined by the RSM model

4. Results and discussion

4. 1. Mean flow field

The mean velocities (axial U, radial V, and tangential W) at the burner outflow for the station's Z/D = 0.3, 0.6, 0.8, 1.0, 1.2, and 1.4 are distributed radially in Figures 5a, 7a, and 8a. The radial velocity (V) is obtained at the station's Z/D = 0.25, 1.0, 1.75, and 2.50. The calculation results are simulated by the RSM turbulence model, combined with the Eddy Dissipation combustion model and the PDF model. Figure 5b dipects the mean axial velocity contours, calculated by the turbulent dissipation combustion model and the RSM turbulence model with a two-step reaction scheme (RSMR2)

on the X=0 plane. Without a doubt, this proves that the presence of the center recirculation zone is responsible for the stabilization of the flame. This flame stabilization is achieved by recycling hot gases and providing a continuous source of radicals (OH, H, O) and heat, as well as the swirling jet (SJ), which improves turbulent mixing and reduces pollutant emissions, ensuring both efficient and clean combustion.

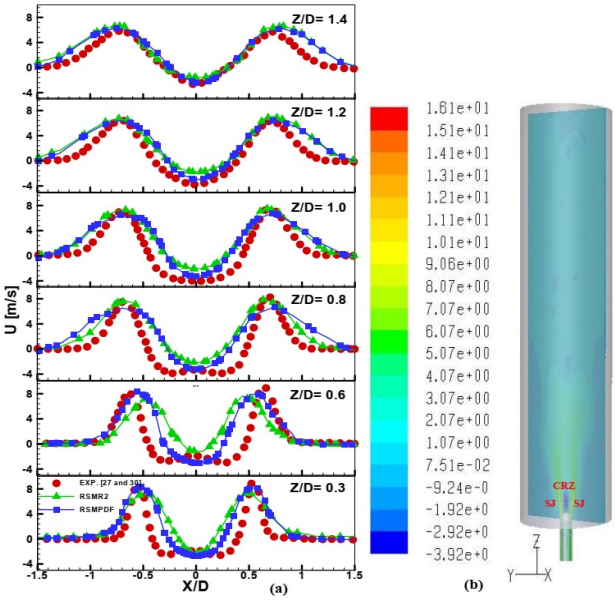

Figure 5. Mean axial velocity: **(a)** Radial distribution of profiles at different stations Z/D = 0.3, 0.6, 0.8, 1.0, 1.2, and 1.4 at the burner outlet. **(b)** Contour of U on the X=0plane

Figure 5a shows the analysis of the radial profiles of the mean axial velocity (U). We observed that the reveal had two distinct flow features characteristic of swirling combustion. First, a high momentum swirling jet (SJ) with peak velocities of about 8 m/s at intermediate radial positions (r/D ≈ 0.2-0.4). Second, a well-defined central recirculation zone (CRZ) characterized by sustained negative velocities (up to -4 m/s) along the flame centerline. While both the Eddy dissipation (R2) and PDF combustion models successfully capture the general behavior of the swirling jet, a critical divergence emerges in their prediction of CRZ characteristics. The PDF model demonstrates remarkable accuracy in simulating CRZ dynamics, maintaining relative errors below 3.5% at downstream stations , whereas the Eddy dissipation (R2) model shows substantial discrepancies exceeding 35% at these locations. This performance gap fundamentally originates from their contrasting treatment of turbulence-chemistry interactions, the transported PDF method explicitly resolves finite-rate chemical effects and turbulent fluctuations through its stochastic fields approach, while the EDM's inherent assumption of infinitely fast chemistry proves inadequate for representing the complex vortex structures and local extinction phenomena within the CRZ [24,26,27,30]. The persistent negative axial velocities observed throughout all prediction's stations (Figure 5b) confirm the CRZ's crucial role in flame stabilization, where it facilitates two key mechanisms: recirculation of hot combustion products to maintain continuous ignition, and enhanced turbulent mixing between fresh reactants and burned gases, thereby optimizing combustion efficiency.

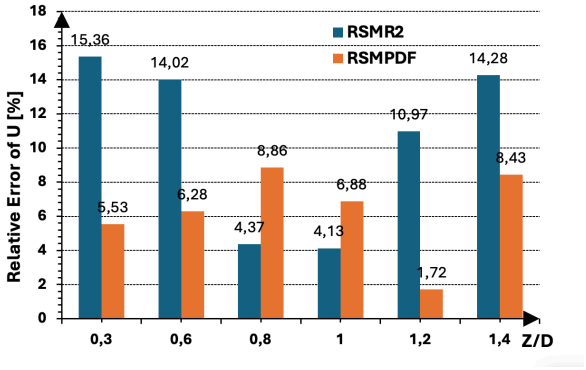

Figure 6. Relative error of the meanaxial velocity predicted with two models RSMR2 and RSMPDF in the swirling jet zone

Figure 6 compares the relative error of the mean axial velocity (U) predicted by the RSMR2 and RSMPDF models in the swirling jet zone. The RSMPDF model shows better accuracy at stations Z/D = 0.3, 0.6, 1.2, and 1.4, with relative errors between 1.72 % and 8.43 %. In contrast, RSMR2 underestimates the experimental data at stations Z/D = 0.3 and 0.6 and overestimates it at stations Z/D = 1.2 and 1.4, with errors ranging from 10.97 % to 15.36 %. At stations Z/D = 0.8 and 1.0, RSMR2 is more accurate (4.37% and 4.13 %), while RSMPDF slightly underestimates (8.86% and 6.88 %). The overall improvement of RSMPDF is due to a better consideration of turbulent fluctuations and turbulence-chemistry interactions via the PDF method. This confirms the superiority of the PDF model in predicting the complex dynamics of the swirling jet, particularly in zones where turbulence and mixing effects are dominant.

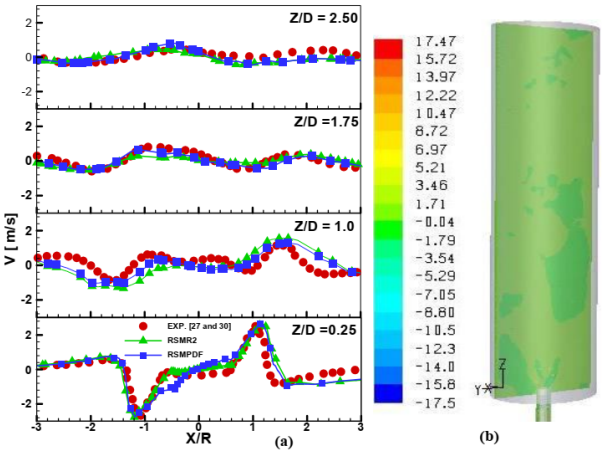

Figure 7. Mean radial velocity: **(a)** Radial distribution of profiles at different stations Z/D = 0.3, 0.6, 0.8, 1.0, 1.2, and 1.4 at the burner outlet. **(b)** Contour of V on the X=0plane

Figures 7b and 8b show the contours of the mean radial and tangential velocities along the Y-Z plane in the combustion chamber, respectively, indicating the presence of the CRZ.

For the comparison of the mean radial velocity profiles (Figure 7a) reveals two distinct flow regimes: a radial expansion (V>0) driven by dominant centrifugal swirl forces at intermediate positions (r/D≈0.5), and an axial recirculation zone (V<0) induced by counter-pressure generated by rotation. The radial velocity profiles indicate that both the PDF and EDM combustion models slightly underestimate the experimental data at the Z/D = 1.0 station. However, at downstream positions (Z/D=0.25,1.75,and 2.5), the results align well with experimental measurements, with the PDF model demonstrating better agreement than the Eddy dissipation two-step reaction(R2) model. The PDF model reproduces these phenomena with an error of less than 5%, compared to the Eddy dissipation model (EDM), which overestimates turbulent diffusion (errors exceeding 25%). This difference is explained by the PDF model's ability to resolve turbulence-chemistry correlations through its joint PDF, which is critical for predicting fine vortex structures (Figure 7b). As for the tangential velocity profiles (Figure 8a) demonstrate that the RSMPDF and RSMR2 combustion models yield comparable predictions, closely matching experimental measurements at burner outlet stations Z/D = 0.3,0.6,and 0.8. Both models accurately replicate experimental profiles, though minor differences in peak positions are observed at the final three stations, with peak values remaining well-predicted. At Z/D = 1.0, the experimental profile exhibits two distinct peaks (X/D = 0.32 and 0.58), corresponding to the shear layer and free-swirling regimes.

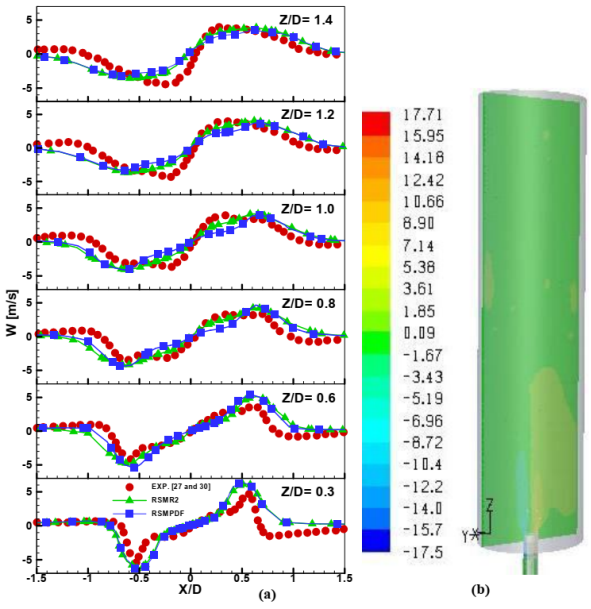

Figure 8. Mean tangential velocity: **(a)** Radial distribution of profiles at different stations Z/D = 0.3, 0.6, 0.8, 1.0, 1.2, and 1.4 at the burner outlet **(b)** Contour of W on the X=0plane.

The RSMPDF model outperforms RSMR2, achieving errors below 4% for both centerline and outer peak predictions, compared to RSMR2's 15% errors. This superior accuracy results from RSMPDF's advanced stochastic modeling of turbulence-chemistry-rotation interactions. Despite slight positional deviations at downstream stations, both models effectively capture the essential dynamics of swirling flow [24,27,30].

4. 2. Temperature field

Figure 9 Depicts the Z-axis radial distribution of mean temperature. The 3D numerical simulation, combining the RSM turbulence model with a two-step reaction scheme, reveals a hot central flame core within the inner recirculation zone. This core is formed by hot intermediate products transported by the flame and extends from the inlet to a distance of 80 mm ~ 95 mm, with a maximum flame temperature reaching approximately 1800 °C. These results confirm those of Mansouri et al. [27]. Combustion completes in this zone, with most combustion gases recirculating in the outer zone.

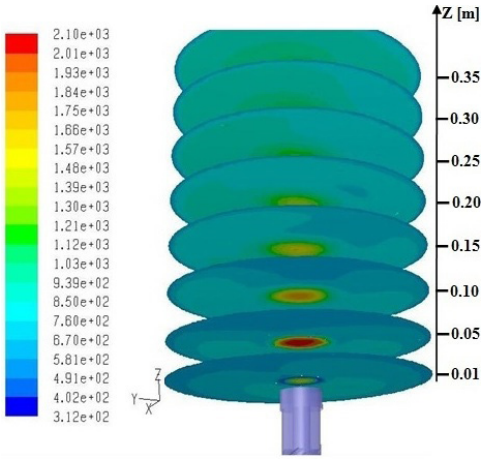

Figure 9. 3D Radial contours of temperature (in K) determined by the RSMR2 model

The radial distribution profiles of mean temperature (Figure 10a) are compared between two combustion models: the PDF turbulence model with a quasi-global reaction scheme (9 species, 8 reactions) and the Eddy dissipation model (EDM) with a simplified scheme (6 species, 2 reactions). Numerical results, incorporating a symmetry condition, align with experimental temperature measurements by Mensouri et al. [27] in a half-domain of the flame. Both models capture the general characteristics of the measured profiles, with distinct performance in predicting peak and downstream temperatures.

At the flame centerline (X/D = 0), temperatures peak between 1500 °C and 1700 °C, reflecting the intense combustion in the central core. At Z/D = 1.25, the RSMPDF model predicts a peak temperature of 1625.19 °C, with a relative error of 1.07% compared to the experimental reference of 1607.94 °C [27]. In contrast, the Reynolds stress model combined with the Eddy dissipation model (RSMR2)

predicts 1673.39 °C, with a higher relative error of 4.07%. These results highlight the PDF model's superior accuracy in capturing finite-rate chemistry effects in the flame core, where swirling-stabilized combustion is most intense.

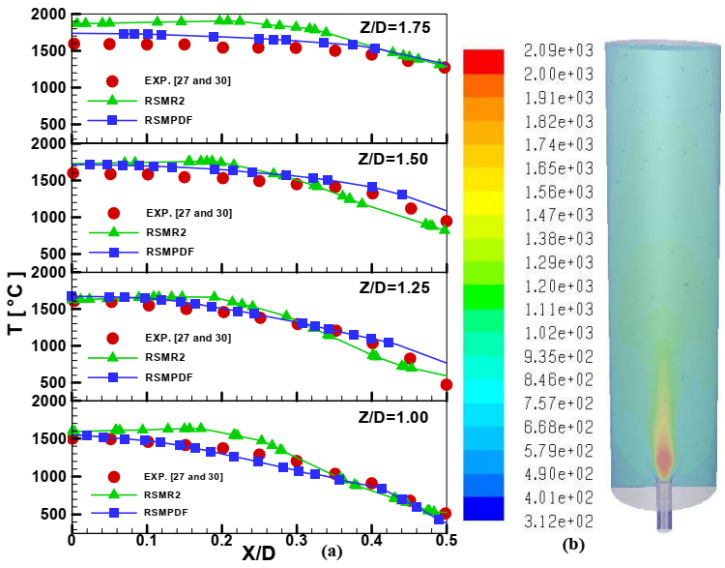

Figure 10. Mean temperature field: **(a)** Radial distribution of profiles at different stations Z/D = 1.0, 1.25, 1.50, and 1.75 at the burner outlet. **(b)** 3D contours of temperature (in K) determined by the RSMPDF model on the X=0 plane

Further downstream, at Z/D = 1.75, both models overestimate temperatures at the burner outlet, but the RSMPDF model performs better, with a relative error of 7.45% compared to the RSMR2 model's 17.25%. The temperature decay to 500-700 °C at this position indicates a transition to a mixing –dominated flow regime. The PDF model's enhanced accuracy arises from its ability to resolve key phenomena, including radiative heat losses via soot prediction and turbulent dissipation of the hot core. Conversely, the EDM's higher error reflects its limitations in modeling complex energy transfer mechanisms, particularly in regions dominated by turbulent mixing and heat loss [27].

Figure 10b shows the contours of the mean temperatures determined by the RSM model and the PDF combustion model along the Y-Z plane in the combustion chamber. The central recirculation zone (CRZ), the transport of hot intermediate products and the conclusion of the combustion process at a peak temperature of approximately 1800 °C are successfully predicted by both models the outer zone is formed by the flow of burnt gases. In this study, the CRZ is correctly predicted by the PDF combustion model, as shown by the radial temperature profiles, and confirmed by results of relative errors of temperature along the centerline (see figure 11).

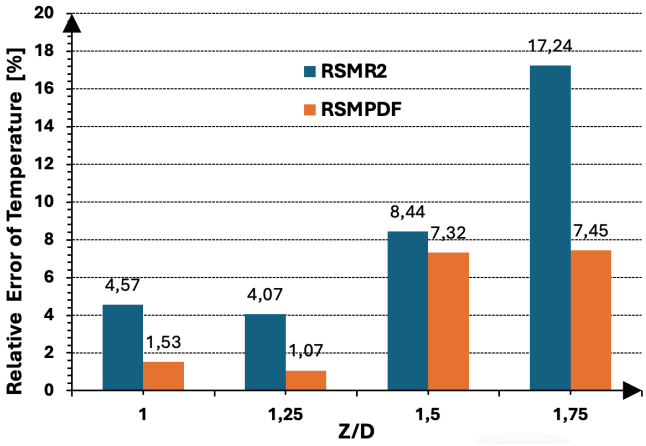

Figure 11. Relative error of the mean temperature calculated along the centerline of the flame predicted with two models RSMR2 and RSMPDF

A comparison of the predicted and experimental findings of the temperature along the centerline of the high-temperature core of the flame is shown in Figure 11. These results were obtained using the two models RSMR2 and RSMPDF. The RSMPDF model correctly estimates maximum temperature values along the centerline, with a minimum relative error of 1.07 % at station Z/D = 1.25 and a maximum of 7.45 % at Z/D = 1.75. In contrast, the RSMR2 model overestimates maximum temperature values, with a minimum relative error of 4.07 % at station Z/D = 1.25 and a maximum of 17.24 % at Z/D = 1.75. These results confirm that the RSMPDF model can predict the maximum temperature values of the flame's hot core as well as micro-mixing effects.

4. 3. Mass fraction of chemical species

Figure 12 illustrates three-dimensional representations of the mean mass fraction distribution of combustion species: (a) methane, (b) oxygen, (c) carbon dioxide, and (d) carbon monoxide. In the core of the combustor, the swirling air jet is responsible for the quick transportation of the radial methane jet across it, where it is quickly consumed through the combustion process. The distributions of Y_{CO_2} exhibit similarities to those of Y_{O_2}, with inverted profiles. The highest concentration of Y_{CO_2} is noted in the central recirculation zone, corresponding with the zero contours of Y_{O_2}. indicating that the central recirculation zone is saturated with combustion products, with no ingress of fresh gas.

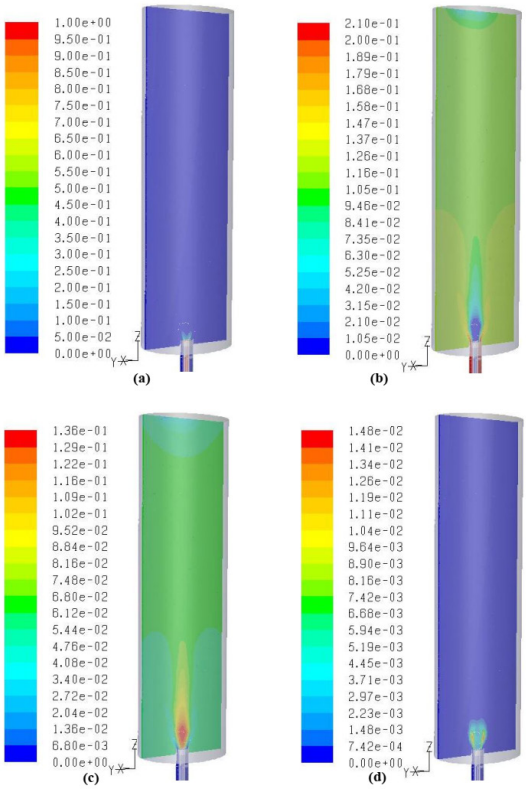

Figure 12. 3D View of the mass fraction distribution of chemical species: **(a)**, **(b)**, **(c)**, and **(d)** CO at the burner outlet along the Z-Y plane

The distribution of Y_{CO} is differs from that of the other species and takes on a V-shape. This distribution is comparable to the contour exposed in Figure 5b, with maximum concentrations of carbon dioxide found in the shear layers of the swirling jet (SJ) region. The mass fraction contour of H_2O (see Figure 13) behaves similarly to the Y_{CO_2} contour.

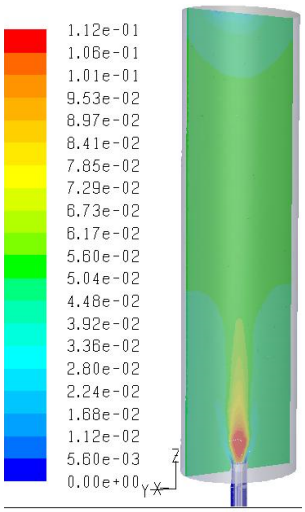

Figure 13. 3D View of the mass fraction distribution of the chemical species H2O at the burner outlet along the Z-Y plane

5. Conclusion

This study is based on a complete numerical analysis of the combustion process of a diffusion flame in a confined, radially fuel-injected coaxial burner. The main purpose is to examine the influence of chemical reaction mechanisms specifically a simplified two-step scheme (6 species, 2 reactions) and a detailed scheme (9 species, 8 reactions) on flame structure, thermal distribution, and stability. The analysis was performed using three-dimensional (3D) simulations based on the RSM model, coupled with two combustion models: the Eddy Dissipation Model (EDM) and the PDF model.

Key work findings include:

- Flow field prediction: The simulations accurately reproduced the central recirculation zone, an essential feature in swirl-stabilized flames. The PDF model demonstrated improved performance in capturing the CRZ's size and location, showing strong agreement with experimental results and corroborating previous work by Khelil et al. [21].
- Velocity profiles: Radial distributions of mean axial, radial, and tangential velocities confirmed the presence of the CRZ, with negative axial velocity values in the core region. Both combustion models successfully replicated these velocity trends.
- Temperature distribution: The PDF model provided more accurate temperature predictions than the EDM model, particularly in the flame core. At Z/D = 1.25, predicted peak temperatures were 1625.19 °C (RSM-PDF) and 1673.39 °C (RSM-EDM), corresponding to relative errors of 1.07% and 4.07%, respectively, when compared to experimental data (1607.94 °C). The temperature profiles further highlighted the differences in model fidelity, particularly in the fuel–oxidizer mixing zone.
- Flame stability: The use of the detailed reaction mechanism with the PDF model led to enhanced flame stability, as indicated by the improved agreement between predicted and experimental temperature peaks within the internal recirculation zone.
- Chemical species concentration: The spatial distributions of major species mass fractions were consistent with the thermal and velocity fields, supporting the reliability of the simulations in capturing the combustion process dynamics.

In summary, this study advances the understanding of turbulence chemistry interactions in diffusion, high-swirl flames. It demonstrates that the RSM–PDF model combination, especially when used with a detailed chemical scheme, offers improved predictive capability for flow, temperature, and species fields. Integrating radiation heat transfer and soot formation models may further improve simulation fidelity.

Acknowledgement

LCTMMS's head offered the laboratory needed for the study.

Author contributions statement

S. Nechad, and A. Khelil: Conceptualization, Investigation, reviewing, writing original draft, Editing and Supervision; M. Braikia: reviewing, writing original draft, Editing and Supervision; Y. Bouhmidi: Analysis and Reviewing.

Declaration of interests

The authors of this study state that there are no conflicts of interest that are associated with the research, authorship, or publication of this manuscript under consideration.

Declaration of generative AI and AI-assisted technologies in the writing process

No generative AI or AI-assisted technologies were used in the preparation of this manuscript.

Nomenclature

A,B	Constants of the Magnussen model
CH_4	Methane
C_2H_6	Ethane
C_3H_8	Propane
C_4H_{10}	Butane
CO	Carbon monoxide
D	Outer diameter of the co-axial tube
D_h	Inner diameter of the central tube
D_{hyd}	Hydraulic diameter
f	The mixture fraction
G_x	Axial momentum flux
G_θ	Tangential momentum flux
h	Distance of the swirler position above the burner exit plane
H_2	Hydrogen
I_{tur}	Turbulent intensity
$M_{\omega,j}$	Molecular weight of species i
N_2	Nitrogen
NO_x	Nitrogen oxides
O_2	Oxygen
P	Pressure
P_{ij}	Production term
R	Characteristic radius
R_e	Reynolds number
R_h	Radii of the hub of the blade
s	Blade thickness
S_f	The source term
S_n	Swirl number
T	Temperature
U	Axial velocity
V	Radial velocity
W	Tangential velocity
Y_c	Mass fraction of a reactant species c
Y_i	Mass fraction for species i
Y_p	Mass fraction of any product species p
z	Number of blades
X,Y,Z	Cartesian coordinates

Greek symbols

ε	Turbulent dissipation rate
k	Turbulent kinetic energy
$\nu_{i,r}$	Stoichiometric coefficient of species i in reaction r
μ	Dynamic viscosity
μ_t	Turbulent viscosity
ρ	density
ψ	Blockage factor
α	The vane angle
Φ	Global equivalence ratio

Subscripts

i,j,k	Coordinate alternation indices
t	Turbulent
$(\bar{..})$	Mean quantity
$(\tilde{..})$	Favre-averaged quantity
$(..)''$	Fluctuations quantity

Abbreviations

CFD	Computational fluid dynamics
CRZ	Central recirculation zone
EBU	Eddy break-up
EDM	Eddy dissipation model
PDF	Probability density function
RANS	Reynolds- averaged Navier-Stokes
RSM	Reynolds stress model
RSMR2	Reynolds stress turbulence model with two-stage reaction scheme
RSMPDF	Reynolds stress turbulence model with probability density function model
SJ	Swirling jet

References

[1] Dewangan SK, Naik MPK, Deshmukh V. Parametric Study of The Non-Premixed Coal Combustion in Furnace for Heat Transfer and Emission Characteristics. J Therm Eng 2020; 6:323–53. https://doi.org/10.18186/THERMAL.833556.

[2] Kumar Y, Qayoum A, Saleem S, Mir FQ. Combined effect of upstream ramp and effusion cooling in combustion chamber liners of gas turbine. J Therm Eng 2023; 9:297–312. https://doi.org/10.18186/thermal.1283203.

[3] Sahu AK, Ghose P. No formation and its reduction through co-flow methane reburn in a pulverised coal combustion process under various overall equivalence ratio. J Therm Eng 2021; 7:2001–16. https://doi.org/10.18186/THERMAL.1051294.

[4] Abay K, Colak U, Yüksek L. Computational fluid dynamics analysis of flow and combustion of a diesel engine. J Therm Eng 2018; 4:1878–95. https://doi.org/10.18186/journal-of-thermal-engineering.388333.

[5] Rather MA, Wani MM. Effect of steam addition on the combustion, performance and emissions characteristics of an HCCI diesel engine. J Therm Eng 2024; 10:710–21. https://doi.org/10.14744/thermal.0000820.

[6] Manickam B. A comparative study of different reaction models for turbulent methane / hydrogen / air 2015; 1:367–80.

[7] Laubscher R, Hoffmann JH. Utilization of basic multi-layer perceptron artificial neural networks to resolve turbulent fine structure chemical kinetics applied to a CFD model of a methane/air piloted jet flame. J Therm Eng 2018; 4:1828–46. https://doi.org/10.18186/journal-of-thermal-engineering.381838.

[8] Al-Mawali J, Dakka SM. Numerical Analysis of Flame Characteristics and Stability for Conical Nozzle Burner. J Therm Eng 2019; 5:422–45. https://doi.org/10.18186/THERMAL.624070.

[9] Gran IR, and Magnussen BF. A Numerical Study of a Bluff-Body Stabilized Diffusion Flame. Part 2. Influence of Combustion Modeling and Finite-Rate Chemistry. Combust Sci Technol 1996; 119:191–217. https://doi.org/10.1080/00102209608951999.

[10] Meier W, Keck O, Noll B, Kunz O, Stricker W. Investigations in the TECFLAM swirling diffusion flame: Laser Raman measurements and CFD calculations. Appl Phys B 2000; 71:725–31.

[11] Faravelli T, Bua L, Frassoldati A, Antifora A, Tognotti L, Ranzi E. A new procedure for predicting NOx emissions from furnaces. Comput Aided Chem Eng 2000; 8:859–64. https://doi.org/10.1016/S1570-7946(00)80145-5.

[12] Frassoldati A, Frigerio S, Colombo E, Inzoli F, Faravelli T. Determination of NOx emissions from strong swirling confined flames with an integrated CFD-based procedure. Chem Eng Sci 2005; 60:2851–69. https://doi.org/https://doi.org/10.1016/j.ces.2004.12.038.

[13] Schmittel P, Günther B, Lenze B, Leuckel W, Bockhorn H. Turbulent swirling flames: Experimental investigation of the flow field and formation of nitrogen oxide. Proc Combust Inst 2000; 28:303–9. https://doi.org/10.1016/S0082-0784(00)80224-6.

[14] Beck CH, Koch R, Bauer H-J. Identification of droplet burning modes in lean, partially prevaporized swirl-stabilized spray flames. Proc Combust Inst 2009; 32:2195–203. https://doi.org/https://doi.org/10.1016/j.proci.2008.06.030.

[15] Pope SB. PDF methods for turbulent reactive flows. Prog Energy Combust Sci 1985; 11:119–92.

[16] Xu J, Pope SB. PDF calculations of turbulent nonpremixed flames with local extinction. Combust Flame 2000; 123:281–307. https://doi.org/https://doi.org/10.1016/S0010-2180(00)00155-3.

[17] Liu K, Pope SB, Caughey DA. Calculations of bluff-body stabilized flames using a joint probability density function model with detailed chemistry. Combust Flame 2005; 141:89–117. https://doi.org/10.1016/j.combustflame.2004.12.018.

[18] Repp S, Sadiki A, Schneider C, Hinz A, Landenfeld T, Janicka J. Prediction of swirling confined diffusion flame with a Monte Carlo and a presumed-PDF-model. Int J Heat Mass Transf 2002; 45:1271–85. https://doi.org/https://doi.org/10.1016/S0017-9310(01)00243-5.

[19] Khelil A, Nechad S, Naji H, Loukarfi L, Braikia M, Beriache M. Numerical study of the influence of combustion models and kinetic schemes when predicting the diffusion flames. J Mech 2012; 28:701–13. https://doi.org/10.1017/jmech.2012.108.

[20] Zhou X, Sun Z, Brenner G, Durst F. Combustion modeling of turbulent jet diffusion H2/air flame with detailed chemistry. Int J Heat Mass Transf 2000; 43:2075–88. https://doi.org/https://doi.org/10.1016/S0017-9310(99)00293-8.

[21] Khelil A, Naji H, Loukarfi L, Mompean G. Prediction of a high swirled natural gas diffusion flame using a PDF model. Fuel 2009; 88:374–81. https://doi.org/https://doi.org/10.1016/j.fuel.2008.09.008.

[22] German AE, Mahmud T. Modelling of non-premixed swirl burner flows using a Reynolds-stress turbulence closure. Fuel 2005; 84:583–94. https://doi.org/https://doi.org/10.1016/j.fuel.2004.10.015.

[23] Boushaki T, Koched A, Mansouri Z, Lespinasse F. Volumetric velocity measurements (V3V) on turbulent swirling flows. Flow Meas Instrum 2017; 54:46–55. https://doi.org/https://doi.org/10.1016/j.flowmeasinst.2016.12.003.

[24] Boushaki T, Merlo N, Chauveau C, Gökalp I. Study of pollutant emissions and dynamics of non-premixed turbulent oxygen enriched flames from a swirl burner. Proc Combust Inst 2017; 36:3959–68. https://doi.org/10.1016/j.proci.2016.06.046.

[25] Merlo N, Boushaki T, Chauveau C, De Persis S, Pillier L, Sarh B, et al. Experimental study of oxygen enrichment effects on turbulent non-premixed swirling flames. Energy and Fuels 2013; 27:6191–7. https://doi.org/10.1021/ef400843c.

[26] Merlo N, Boushaki T, Chauveau C, Persis S De, Pillier L, Sarh B, et al. Combustion characteristics of methane-oxygen enhanced air turbulent non-premixed swirling flames. Exp Therm Fluid Sci 2014; 56:53–60. https://doi.org/10.1016/j.expthermflusci.2013.11.019.

[27] Mansouri Z, Boushaki T. Experimental and numerical investigation of turbulent isothermal and reacting flows in a non-premixed swirl burner. Int J Heat Fluid Flow 2018; 72:200–13. https://doi.org/10.1016/j.ijheatfluidflow.2018.06.007.

[28] Ferziger JH, Perić M. Computational methods for fluid dynamics. Springer; 2002.

[29] Poinsot T, Veynante D. Theoretical and numerical combustion. RT Edwards, Inc.; 2005.

[30] Merlo N. Caractérisation expérimentale d'une flamme turbulente non prémélangée swirlée : effet de l'enrichissement en oxygène. Université d'Orléans, 2014.

[31] Chen F, Liu H. Particle image velocimetry for combustion measurements: Applications and developments. Chinese J Aeronaut 2018; 31:1407–27. https://doi.org/10.1016/j.cja.2018.05.010.

[32] Mansouri Z, Aouissi M, Boushaki T. Detached Eddy Simulation of High Turbulent Swirling Reacting Flow in a Premixed Model Burner. Combust Sci Technol 2016; 188:1777–98. https://doi.org/10.1080/00102202.2016.1211888.

[33] Badiger S, Katti V V., Anil TR. Experimental investigation of heat transfer characteristics of an inverse diffusion flame in a coaxial tube burner for with and without swirl. J Therm Eng 2022; 8:67–77. https://doi.org/10.18186/thermal.1067021.

[34] Esquiva-Dano I, Nguyen HT, Escudie D. Influence of a bluff-body's shape on the stabilization regime of non-premixed flames. Combust Flame 2001; 127:2167–80. https://doi.org/https://doi.org/10.1016/S0010-2180(01)00318-2.

[35] Tong Y, Liu X, Wang Z, Richter M, Klingmann J. Experimental and numerical study on bluff-body and swirl stabilized diffusion flames. Fuel 2018; 217:352–64. https://doi.org/10.1016/j.fuel.2017.12.061.

[36] Sudarma AF, Al-Witry A, Morsy MH. Rans numerical simulation of lean premixed bluff body stabilized combustor: Comparison of turbulence models. J Therm Eng 2017; 3:1561–73. https://doi.org/10.18186/journal-of-thermal-engineering.353668.

[37] Kazanc\i OV, Böke YE. Validation of Bluff-body Swirling Flame with RANS Turbulent Model and Comparison of the Results with LES Turbulent Model. Int J Thermodyn 2024; 27:59–74.

[38] Khelil A, Naji H, Braikia M, Loukarfi L. Comparative investigation on heated swirling jets using experimental and numerical computations. Heat Transf Eng 2015; 36:43–57. https://doi.org/10.1080/01457632.2014.906279.

[39] Nechad S, Khelil A, HadjMeliani M, Loukarfi L, Braikia M. Three-dimensional numerical investigation on swirling jets and elliptic jets with different aspect ratio. Struct Integr LIFE-INTEGRITET I VEK Konstr 2018; 18:197–205.

[40] Dash SC, Singh N. Study of axisymmetric nature in 3-D swirling flow in a cylindrical annulus with a top rotating lid under the influence of axial temperature gradient or axial magnetic field. J Therm Eng 2017; 3:1588–606. https://doi.org/10.18186/journal-of-thermal-engineering.353737.

[41] Khelil A, Naji H, Loukarfi L, Meliani MH, Braikia M. Numerical simulation of the interactions among multiple turbulent swirling jets mounted in unbalanced positions. Appl Math Model 2016; 40:3749–63. https://doi.org/10.1016/j.apm.2015.10.047.

[42] Kaplan S, Bayramoğlu K, Sarikanat M, Altay L. Numerical study on heat transfer and fluid dynamics in plate heat exchangers: Effects of chevron angle and aspect ratio. J Therm Eng 2024; 10:638–56. https://doi.org/10.14744/thermal.0000816.

[43] Zahout N, Braikia M, Khelil A, Naji H. Thermal and dynamic characterization of a multi-jet system with different geometry diffusers. J Therm Eng 2024; 10:404–29. https://doi.org/10.18186/thermal.1456643.

[44] Hasan KS. Experimental study on the combustion of gaseous based fuel (LPG) in a tangential swirl burner of a steam boiler. J Therm Eng 2024; 10:1226–40. https://doi.org/10.14744/thermal.0000863.

[45] Ma L, Li K, Fang Q, Chen G, Zhang C. A novel swirl burner with coal co-firing ammonia: Effect of extension length of the dual-channel ammonia pipe on combustion and NOx formation. Int J Hydrogen Energy 2024; 78:344–52. https://doi.org/https://doi.org/10.1016/j.ijhydene.2024.06.293.

[46] Mahmood AS, Saleh FA. Flame Stability in Swirling and Bluff-Body Burners: a Review. J Teknol 2023; 85:1–15. https://doi.org/10.11113/jurnalteknologi.v85.19588.

[47] Mahmood AS, Saleh FA. Experimental Study of the Effect of Swirl Number and Bluff Body Size on the Stability Map of Premixed LPG Flames in a Tangential Swirl Burner. Jordan J Mech Ind Eng 2023; 17:595–604. https://doi.org/10.59038/jjmie/170414.

[48] Mahmood AS, Saleh FA. Study of the Impact of LPG Composition on the Blowoff and Flashback Limits of a Premixed Flame in a Swirl Burner. J Appl Fluid Mech 2024; 17:616–27. https://doi.org/10.47176/jafm.17.3.2175.

[49] Eldrainy YA, Saqr KM, Aly HS, Jaafar MNM. CFD insight of the flow dynamics in a novel swirler for gas turbine combustors. Int Commun Heat Mass Transf 2009; 36:936–41. https://doi.org/10.1016/j.icheatmasstransfer.2009.06.013.

[50] Gang L, Yujun Z, Cunxi L, Xi J, Qi C, Gang X, et al. The design and characteristics of a novel injector - A lobed swirl injector. Proc ASME Turbo Expo 2017;4A-2017:1–9. https://doi.org/10.1115/GT201763435.

[51] Olivani A, Solero G, Cozzi F, Coghe A. Near field flow structure of isothermal swirling flows and reacting non-premixed swirling flames. Exp Therm Fluid Sci 2007; 31:427–36. https://doi.org/10.1016/j.expthermflusci.2006.05.003.

[52] Flunet. Fluent User's Guide,Version 6.3, Fluent Inc,Lebanon 2004.

[53] Launder BE. Second-moment closure and its use in modelling turbulent industrial flows. Int J Numer Methods Fluids 1989; 9:963–85.

[54] Spalding DB. Mixing and chemical reaction in steady confined turbulent flames. Symp Combust 1971; 13:649–57. https://doi.org/10.1016/S0082-0784(71)80067-X.

[55] Ertesvåg IS, Magnussen BF. The Eddy dissipation turbulence energy cascade model. Combust Sci Technol 2000; 159:213–35. https://doi.org/10.1080/00102200008935784.

[56] Westbrook CK, Dryer FL. Chemical kinetic modeling of hydrocarbon combustion. Prog Energy Combust Sci 1984; 10:1–57. https://doi.org/10.1016/0360-1285(84)90118-7.